Electrochimica Acta 273 (2018) 181–190

Contents lists available at ScienceDirect

Electrochimica Acta

journal homepage: www.elsevier.com/locate/electacta

Low temperature preparation of pore structure controllable graphene for high volumetric performance supercapacitors

Songbo Chen [1], Wensheng Gao [1], Yuanzhi Chao, Yu Ma, Yunhai Zhang, Nan Ren, Huqiang Chen, Lijun Jin, Jiangong Li, Yongxiao Bai*

Institute of Material Science and Engineering, Key Laboratory for Magnetism and Magnetic Materials of the Ministry of Education, Key Laboratory of Special Function Materials and Structure Design of Ministry of Education, Lanzhou University, Lanzhou 730000, China

ARTICLE INFO

Article history:
Received 13 January 2018
Received in revised form
10 March 2018
Accepted 4 April 2018
Available online 5 April 2018

Keywords:
Low temperature process
Pore structure controllable
Graphene
Volumetric capacitance
Supercapacitors

ABSTRACT

High volumetric capacitance of supercapacitor is important and challenging for practical application in the energy storage devices. Herein, we develop a simple and effective approach to fabricate functionalized and pore structure controllable graphene via low temperature (~170 °C) thermal treatment of graphite oxide with designed particle size. The as-obtained graphene with oxygen contents of 14.19 at.%, porous structure and a relative low pore volume (0.38 g cm^{-3}), exhibits a promising material for the application in high volumetric performance supercapacitors. The prepared supercapacitor delivers a high volumetric capacitance of 226.9 F cm^{-3} at 0.5 A g^{-1} and achieves high rate capability (79% capacitance retention at 20 A g^{-1}) in alkaline electrolyte. Moreover, the assembled supercapacitor in neutral electrolyte also exhibits a high volumetric energy density of 15.1 Wh L^{-1} as well as a high cycling stability with 94.2% retention after 9000 cycles. Therefore, this work will provide a new strategy for designing high volumetric capacitive performance of graphene for energy storage devices.

1. Introduction

Supercapacitors (SCs), also called electrochemical capacitors, is regarded as one of the most important energy storage devices owing to their characteristics of high power capability, long cycle life and high reliability [1–3]. SCs store electrical energy either in the electrochemical double layer (EDL) formed by the absorption of electrolyte ions in the surface of the electrode or faradaically by redox reactions occurring in the surface regions of the electrode materials [4–6]. Compared to batteries, SCs have the advantages of high power density, long cycle life but lower energy density [7]. Hence, one of the most critical aspects is the improvement of the energy density without deterioration of the other performance of SCs [8].

Recently, graphene has been widely explored as an appealing electrode material owing to its high specific surface area, high electric conductivity and theoretical specific capacitance (≈550 F g^{-1}) [9–11]. However, the capacitive performance is still limited owing to the re-stacking of graphene layer which reduces the accessible surface area for charge storage during both electrode assembly and cycling [12]. In order to solve this problem, a promising way is to introduce another electroactive species between graphene layers such as conducting polymers [13–15], transition metal oxides [16–18] and oxygen-containing functional groups [19–21], which would not only significantly improve electrolyte accessible surface area of graphene, but also enhance the capacitive performance of the electrode. Moreover, improving the gravimetric capacitance of graphene-based SCs have been mainly considered from many scientific achievements. However, the majority of the results reported for graphene-based SCs were obtained low density electrode materials, which contain large pore volume and result in relative low volumetric capacitance [12,22–24]. Thus, design graphene-based electrode materials with both high gravimetric capacitance and high volumetric capacitance are required for the practical applications where the space is limited [25,26]. So far, many efforts have been focused on fabricate the high volumetric density graphene through different approaches [27–29]. For instance, Fan and co-workers synthesized functionalized graphene via $Mg(OH)_2$ template assistant and low temperature reduction treatment, and the resulting materials exhibited ultrahigh volumetric capacitance performance [24]. The template assistant

* Corresponding author.
E-mail address: baiyx@lzu.edu.cn (Y. Bai).
[1] These authors contributed equally to this work.

https://doi.org/10.1016/j.electacta.2018.04.034
0013-4686/

strategy is complicated and need to post-processing to remove the template. In addition, Li et al. reported the synthesis of oxygen and nitrogen co-doped porous carbon nanosheets by directly pyrolyzing perilla frutescens leaves, and the synthesized carbons showed a high O, N contents and a relatively low pore volume which delivers a high volumetric capacitance [30]. This approach can endow carbon material with heteroatomic doped, but the control of the density of pore structure is also difficult [31–34]. The above works suggest that design carbon materials with surface functional groups coupled with high particle density is an effective strategy to achieve both high gravimetric and volumetric capacitance in aqueous SC applications. Despite many tries have been done, a facial method for preparation of graphene with controllable particle density and functionality density is still a difficult challenge.

In our recent exploration for modified graphene materials, we developed a low temperature thermal reduction method to obtain a kind of graphene materials with surface modification [35]. Such materials demonstrated good dispersibility in polyolefin nanocomposites, but still limit in design high volumetric material owing to the relative high specific surface area and pore volume. To solve above mentioned problems, an optimized low temperature thermal reduction of graphite oxide (LTRGO) method is explored to fabricate controllable meso- and macropore volume through using designed size of graphite oxide as precursor. This low temperature process (about 170 °C) remains a mass of oxygen-containing functional groups, and a series of electrode materials with gradually decreasing of the pore volume has been obtained. Especially, the LTRGO1 prepared with the largest particle size of graphite oxide shows a porous framework, high oxygen contents of 14.19 at.%, and high particle density (up to 1.14 g cm^{-3}). After used as electrode material for SC, the LTRGO1-SC delivers specific capacitance up to 226.9 F cm^{-3} at 0.5 A g^{-1} (199.7 F g^{-1} at 0.5 A g^{-1}) in alkaline electrolyte. More importantly, in the neutral electrolyte, the LTRGO1-SC exhibits a high volumetric energy density (15.1 Wh L^{-1} at 257 W L^{-1}) and a capacitance retention of 94.2% after 9000 cycles at 5 A g^{-1}.

2. Experimental section

2.1. Preparation of LTRGO samples

All of the reagents were analytical pure and they were used without further purification. LTRGO was synthesized by low temperature reduction and exfoliation method with graphite oxide as precursor, as described in our recent paper [35]. Taking the preparation of LTRGO1 as an example, graphite flakes (99 mesh, 25 g) were placed in concentrated H_2SO_4 (500 mL) in a 2 L flask and cooled by an ice bath (<5 °C). While maintaining stirring, $KMnO_4$ (150 g) was gradually added to the solution to keep the temperature below 30 °C. After stirring for 24 h, the mixture was gradually added to deionized water (3 L), and the reaction is finally terminated by the addition of 15% H_2O_2 (50 mL), after which the colour of the solution was changed from black to bright yellow. For purification, the mixture was washed using 5–10% HCl solution and deionized water several times until no sulfate ions detected. After filtration and drying under vacuum at 50 °C for 24 h, graphite oxide was obtained as a brownish black cake, and the GO powder was obtained by mechanical grinding of the GO cake to small pieces.

To prepare LTRGO1 sample, the as-prepared GO powder was placed into a quartz tube in a horizontal furnace which was preheated to 80 °C. One end of the tube was closed using a rubber stopper while the other was sealed with a plastic sealed bag which was used to collect the resultant product. The quartz tube was heated quickly from 80 °C to about 170 °C under 5 min while the GO powder was slightly exploded. The resultant black carbon material was collected directly from a plastic sealed bag and washed with ethanol before drying in an oven at 80 °C for 12 h. Similarly, LTRGO2 and LTRGO3 were obtained just by changing the size of graphite in 325 mesh and 2000 mesh, respectively.

2.2. Characterization methods

The morphologies and microstructures of the obtained samples were characterized by a field emission scanning electron microscopy (FE-SEM, Hitachi S-4800) and transmission electron microscopy (TEM, Talos F200c). The chemical component was analyzed on an ESCALAB 250 multifunctional X-ray photoelectron spectroscope. X-ray diffraction (XRD-Rigaku D/max-2400) was used to carry out the crystallographic structures of the materials. The nitrogen adsorption was measured using a Micromeritics accelerated surface area porosimetry (ASAP 2020, USA) autoadsorption analyzer to obtain N_2 adsorption isotherms at 77 K, and the specific surface area (SSA) was obtained by Brunauer–Emmett–Teller (BET) analyses of the adsorption isotherms. The pore size distribution and pore volume were calculated from Barrett–Joyner–Halenda method for mesopores and macropores. The nature of the bonding was characterized by Raman spectroscope (Horiba Jobin Yvon LABRAM-HR800 with a wavelength range of 0–4000 cm^{-1}).

2.3. Electrochemical measurements

Symmetric two-electrode supercapacitors were assembled to evaluate the supercapacitive performance of the products and the electrochemical performance was tested by cyclic voltammetry (CV), galvanostatic charge-discharge (GCD) and electrochemical impedance spectroscopy (EIS) on a CHI 660 E electrochemical workstation (Chenhua, Shanghai, China) with both 6.0 M KOH and 1.0 M Na_2SO_4 as aqueous electrolytes. Briefly, 80 wt% product, 10 wt % carbon black, and 10 wt% PTFE were mixed into a slurry using an agate mortar and pestle, followed by uniform coating onto nickel foam with a diameter of 1.4 cm and dried at 100 °C for 12 h in a vacuum oven. The symmetric supercapacitor was fabricated with two identical electrodes/collectors in CR2025 stainless steel coin cell with the porous cellulose membrane as separator. The mass loading on each electrode was about 1.5–1.8 mg. The potential range for CV and GCD test was 0–1.0 V (using 6.0 M KOH as electrolyte) and 0–1.8 V (using 1.0 M Na_2SO_4 as electrolyte). EIS test was performed in the frequency range of 100 kHz to 10 mHz at an amplitude of 5 mV. Leakage current was tested using an LANHE instruments testing system. Detailed electrochemical calculations are described in supporting information (SI).

3. Results and discussion

The fabrication processes of LTRGO materials are schematically illustrated in Fig. 1a, similar to our recent works [35]. Firstly, graphite oxide was synthesized by modified Hummers method with different size of graphite (99 mesh, 325 mesh and 2000 mesh) as precursor. In this process, graphite was fully oxidation by the strong oxidizing agents and the interlayer of graphite was intercalated with a mass of oxygen-containing functional groups like oxhydryl, epoxy and carboxyl, etc. Subsequently, for LTRGO1, the reduction and exfoliation process of the graphite oxide (obtained by 99 mesh graphite as precursor, with an average size around 150 μm) were carried out simultaneously with ultrarapid thermal treatment which was preset at 80 °C and heated up rapidly to about 170 °C, thus completing the preparation of LTRGO1. This simple and effective process is used to obtained oxygen-containing functional graphene without hazardous reductant, high vacuum environment assistant or high temperature. As a control, LTRGO2 and LTRGO3

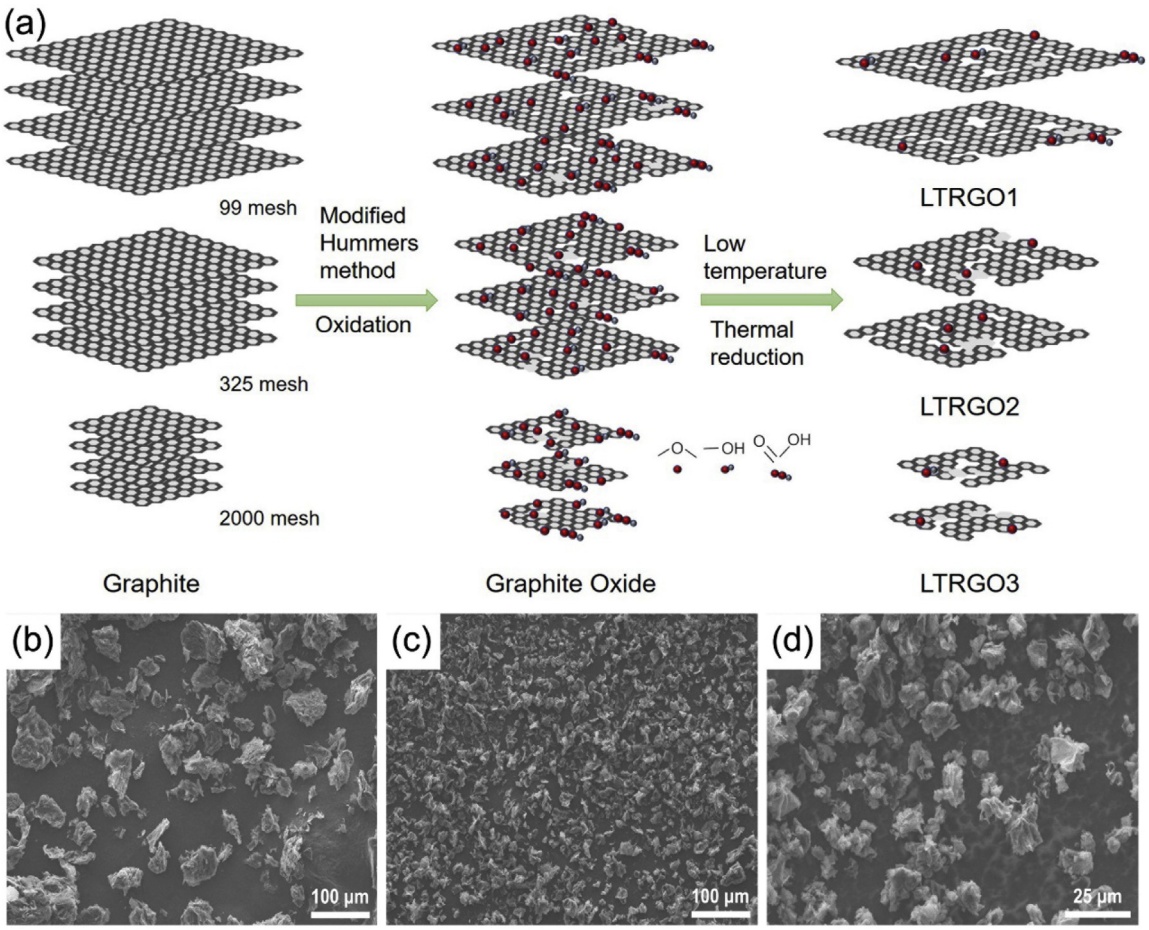

Fig. 1. Preparation and characterization of LTRGO1, LTRGO2, and LTRGO3. (a) Schematic illustration for the fabrication of LTRGO material; (b–d) SEM images of LTRGO1, LTRGO2 and LTRGO3, respectively.

were obtained by changing the size of graphite in 325 mesh (with an average size around 45 μm) and 2000 mesh (with an average size around 6.5 μm), respectively. The low magnification SEM images of the as-prepared samples are shown in Fig. 1b–d. For LTRGO1, the particle size was mainly distributed at dozens of micrometers, larger than that of LTRGO2 (around a dozen of micrometer) and LTRGO3 (less than 10 μm).

The structure of as-prepared LTRGO samples was further characterized by SEM with different magnifications and TEM. As shown in Fig. 2, the as-prepared samples show similar surface morphology with curved edges and the local overlapping (Fig. 2a–c), indicating a compact layered structure after reduction. In addition, the interlayer of sheets still maintains abundant open pores and the layer distance become more and more denser with the decreasing of precursor size of graphite oxide (Fig. 2d–f). The TEM image further indicates that there are numerous functional groups on the surface of sheets before reduction, and the removed of functional groups left 'footprints' which make the as-prepared sheets wrinkled [24]. Interestingly, the curved and agglomerate appearance of the sheets are more and more apparent with diminishing precursor size of graphite oxide (Fig. 2g–i and Fig S1), corroborating higher reduction degree of the smaller size of graphite oxide particle during low temperature reduction process.

The bulk structure of the prepared LTRGO1, LTRGO2 and LTRGO3 were investigated by XRD and Raman spectroscopy and the results are shown in Fig. 3. XRD patterns of all samples exhibit a broad diffraction peak at around 25° (Fig. 3a), ascribing to the (002) crystal planes of graphitic carbon. Interestingly, the (002) peaks for LTRGO1 and LTRGO2 shift to a lower angle compared to that of LTRGO3, revealing a slightly decreased degree of graphitization and crystallinity and this may attribute to the lower reduction degree of the precursor with large size during the rapid reduction process. These phenomena reveal that smaller size of graphite oxide delivers higher reduction degree during the reduction precess owing to the relative higher marginal oxygen-containing functional groups which are beneficial to decompose during the rapid reduction process [36,37]. The Raman spectra further verify the increased defects (I_D/I_G) with elevated the size of the precursor as shown in Fig. 3b. For graphene materials, the D band is a characteristic feature of defects induced in the graphitic structure and functional groups attached on the surface of graphene sheets, while the G band corresponds to sp^2-hybridized graphitic layers [38–40]. Additionally, two broad signals at ~1190 and 1486 cm^{-1} are deconvoluted in the overall Raman spectrum by Origin Software (Gaussian Multi-peaks Fit) [41,42]. These two peaks are attributed to carbon atoms outside of planer graphene and distortions of inner symmetry in aromatic rings, respectively [41–43]. The ratio of integrated intensity (I_D/I_G) of LTRGO1, LTRGO2 and LTRGO3 was calculated to be 0.932, 0.926 and 0.910, respectively. It is worth noting that the I_D/I_G ration for LTRGO1 shows slightly larger than that of LTRGO2 and LTRGO3, thus meaning that higher oxygen-containing functionalities accompanying the recovery of the sp^2 graphitic sheets were obtained during the rapid reduction process [20], which is consist with XPS results as described below.

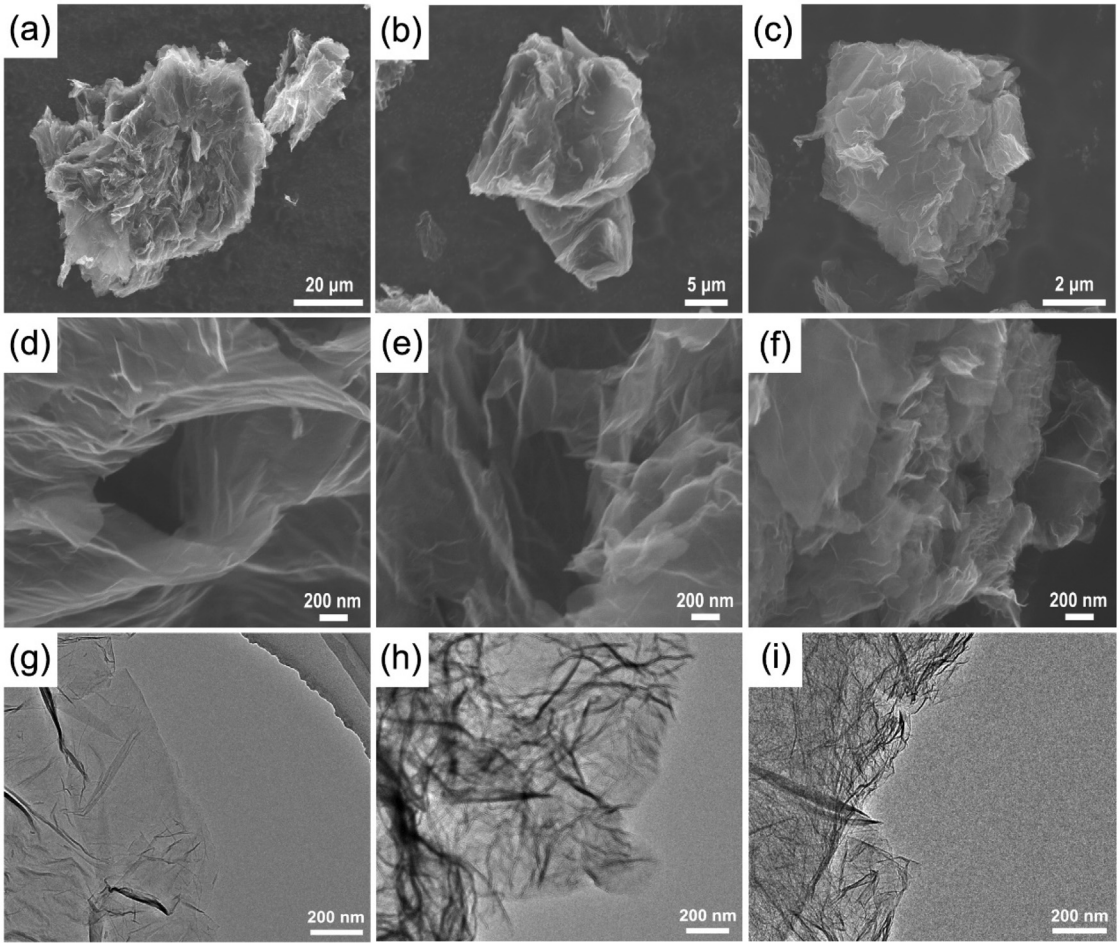

Fig. 2. SEM images of LTRGO1 (a, d), LTRGO2 (b, e) and LTRGO3 (c, f) and TEM images of LTRGO1 (g), LTRGO2 (h) and LTRGO3 (i).

To further illustrate the pore structure of obtained samples, the Brunauer-Emmett-Teller surface area was employed using nitrogen adsorption-desorption measurements. The nitrogen sorption isotherms and pore size distributions of LTRGO1, LTRGO2 and LTRGO3 samples are shown in Fig. 3c and d, respectively. It is clear that all the LTRGO samples show a type IV sorption isotherm and large hysteresis loop at the relative pressure P/P_0 between 0.45 and 1.0, indicating the dominant presence of macropores and mesopores in these samples [44]. BET analysis shows the specific surface area of LTRGO1, LTRGO2 and LTRGO3 are 113 $m^2 g^{-1}$, 239 $m^2 g^{-1}$ and 283 $m^2 g^{-1}$, respectively. The increase in the SSA could attribute to the smaller particle size of graphite oxide driven a slightly higher exfoliation degree than the other samples during the rapid reduction process, consistent with the gradual shrink of the hysteresis areas. These results can also be observed in the Barrett-Joyner-Halenda (BJH) plots, where the LTRGO3 sample shows the highest pore volume than that of others. Also, the BJH pore size distribution indicates a sharp peak at about 3 nm, suggesting well-developed mesopores structure of these samples. The dominant pore size range of these samples is in the range of 2 through 30 nm. The information about pore volume were obtained from BJH method, as shown in the inset of Fig. 3d. The mesopore volume for LTRGO1, LTRGO2 and LTRGO3 are 0.211 $cm^3 g^{-1}$, 0.460 $cm^3 g^{-1}$ and 0.619 $cm^3 g^{-1}$, respectively, indicating the pore structure controllable graphene after the low temperature reduction process. The gradually decreasing of meso- and macropore volumes lead to the prominent increase in the particle density which is beneficial for designing high volumetric electrode material for SC [3]. The textural properties of the LTRGO1, LTRGO2, and LTRGO3 samples are listed in Table 1.

The chemical component and bonding configurations of these samples were further investigated by XPS. In Fig. 4a, all samples exhibit two peaks centered at 284.8 eV and 513.4 eV, corresponding to C 1s and O 1s, respectively. The percentage of oxygen can be calculated to be 14.19 at%, 13.80 at% and 13.33 at% for LTRGO1, LTRGO2 and LTRGO3 samples, respectively, meaning that the oxygen-containing groups can be more effective removed with the gradual decrease of the precursor size of graphite oxide. The O 1s spectra of the samples are shown in Fig. 4b–d and the three peaks centered at 531.2, 532.8 and 533.9 eV are attributed to C=O in quinone or ester, C-O/C-OH in ester or phenol and -COOH groups, respectively [45,46]. Notably, oxygen-containing functional groups not only can provide pseudocapacitance from the redox reactions occurring in the active surface regions of graphene but also improve the wettability between the electrode and electrolyte ions [9,47]. According to the O 1s spectra, the LTRGO1 sample shows the contents of C=O group (51.2%) on graphene sheets higher than that of LTRGO2 (46.6%) and LTRGO3 (43.8%), indicating more pseudocapacitance driven from oxygen-containing functional groups (Table 2). Therefore, the higher O/C ratio of LTRGO1 and the dominant C=O group would deliver more pseudocapacitance among these samples [48], which will be discussed vide infra.

The capacitive behavior of LTRGO samples was explored in a two-electrode system using 6 M KOH as electrolyte. As shown in

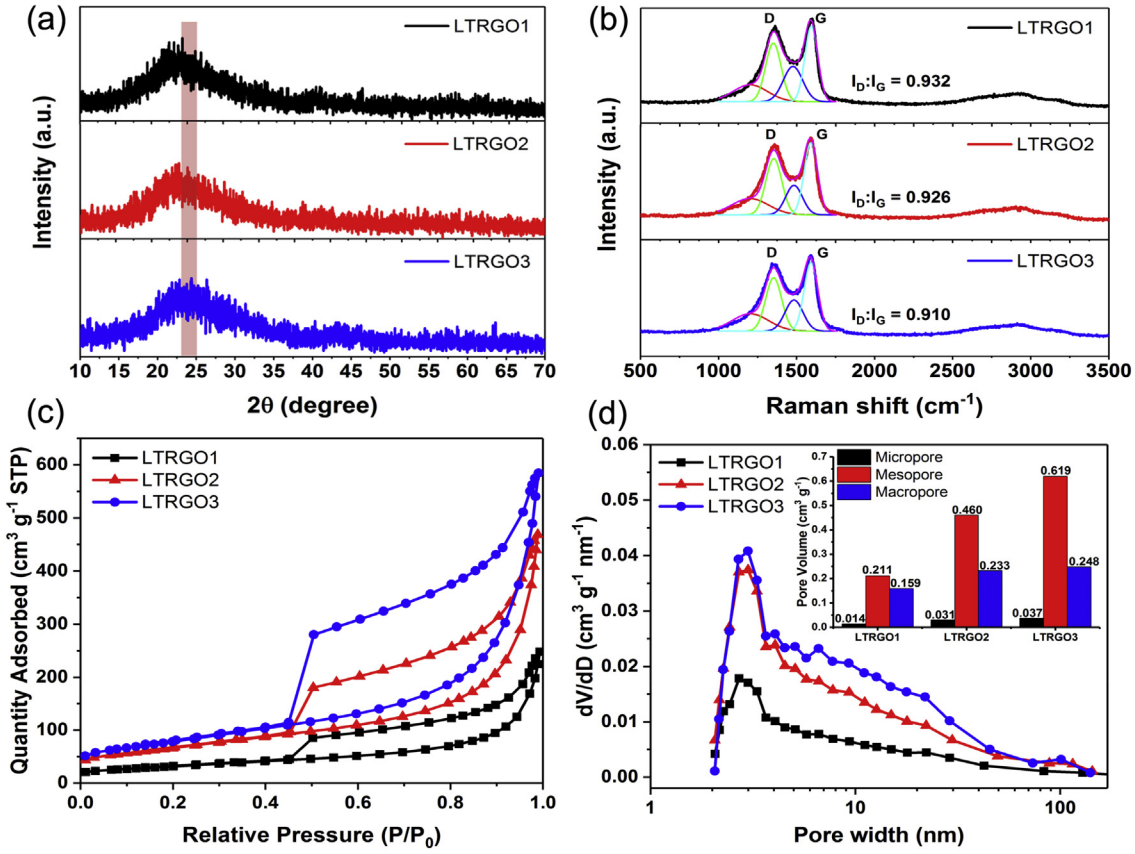

Fig. 3. (a) XRD patterns, (b) Raman spectra, (c) N_2 adsorption/desorption isotherms and (d) Pore size distributions of LTRGO1, LTRGO2 and LTRGO3. Inset shows histograms of micro-, meso- and macropore volumes.

Table 1
Pore structure parameters of LTRGO samples.

Samples	BET SSA ($m^2\ g^{-1}$)			Pore Volume ($cm^3\ g^{-1}$)				Pore Size (nm)[a]	Density (g cm^{-3})[b]
	Total	Micro	External	Total	V_{micro}	V_{meso}	V_{macro}		
LTRGO1	113	57	56	0.384	0.014	0.211	0.159	8.1	1.14
LTRGO2	239	122	117	0.724	0.031	0.460	0.233	7.4	0.82
LTRGO3	283	147	136	0.904	0.037	0.619	0.248	6.1	0.71

[a] Desorption average pore width.
[b] Calculated by Eq (2).

Fig. 5a, CV curves of all LTRGO-SCs at the scan rate of 50 mV s^{-1} exhibit quasi-rectangular shapes with slight distortions, indicating the synergic effects of the EDLC behavior and pseudocapacitive behavior contributed from oxygen-containing redox region. In addition, LTRGO1-SC displays largest specific capacitance, which is indicative of a promising electrode material of the LTRGO1 sample. Notably, the CV curves at different scan rate of the LTRGO1-SC (Fig. 5b) exhibits nearly rectangular-like shapes with broadened peaks even at the high scan rate of 200 mV s^{-1}, demonstrating excellent rate capability and fast charge-propagation capability. To further study the electrochemical behavior, GCD test were employed for all LTRGO-SCs at the current density of 0.5 A g^{-1} and 1 A g^{-1} (Fig. 5c). The specific capacitance of LTRGO1 reaches 199.7 F g^{-1} and 195.7 F g^{-1} at 0.5 A g^{-1} and 1 A g^{-1}, respectively, higher than that of LTRGO2-SC (184.7 F g^{-1} at 0.5 A g^{-1} and 175.8 F g^{-1} at 1 A g^{-1}) and LTRGO3-SC (155.8 F g^{-1} at 0.5 A g^{-1} and 148.9 F g^{-1} at 1 A g^{-1}). The reason for the increased capacitance of LTRGO1-SC is mainly due to the effective redox reactions which deliver higher pseudocapacitance. Moreover, even increasing the current density to 20 A g^{-1}, LTRGO1-SC still maintains a high specific capacitance of 157.9 F g^{-1}, which is about 79% of its initial capacitance at 0.5 A g^{-1} (Fig. 5d and e), higher than that of the LTRGO2-SC (125.7 F g^{-1}) and LTRGO3-SC (98.2 F g^{-1}), demonstrating excellent rate capability. Owing to its relatively high density (1.14 g cm^{-3} calculated by Eq. (2), see SI), the LTRGO1-SC possesses a large volumetric capacitance of 226.9 F cm^{-3} at 0.5 A g^{-1} (Fig. 5e), which is higher than that of the other two SCs (151.4 F cm^{-3} for LTRGO2-SC and 111.3 F cm^{-3} for LTRGO3-SC). The corresponding energy density of LTRGO1-SC, LTRGO2-SC and LTRGO3-SC calculated by Eq. (4,5) are listed in Table S1 (see SI) and this results show that volumetric capacitances of LTRGO1-SC is competitive compared to those advanced carbon materials in aqueous electrolyte (Table S3, see SI). In addition, as shown in fig. S4, owing to the high packing density and functionality, the area-normalized capacitance for LTRGO1-SC is 177 μF cm^{-2}, higher than that of LTRGO2-SC (77 μF cm^{-2}) and LTRGO3-SC (55 μF cm^{-2}).

To further understand the superior performance of LTRGO1-SC, EIS test was also used to reveal the electrolyte ion transport

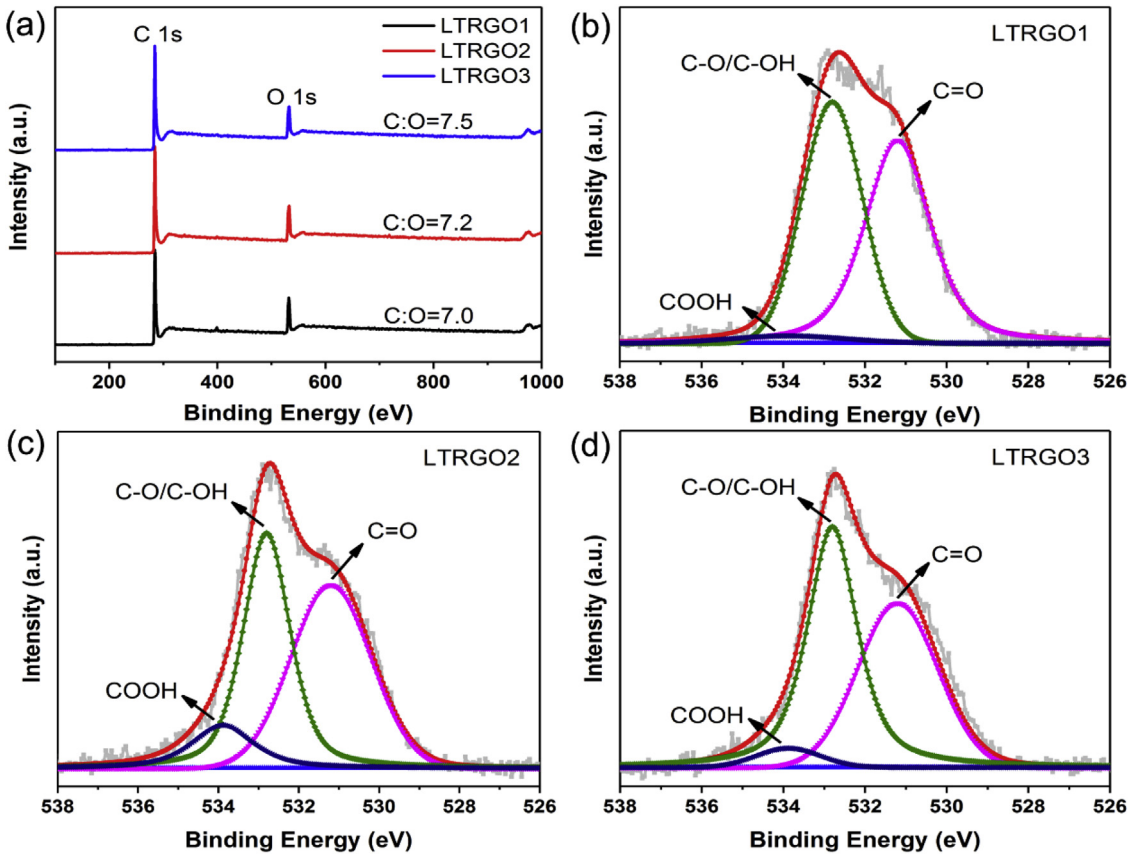

Fig. 4. (a) Full-scale XPS spectra and the O 1s spectra of LTRGO1 (b), LTRGO2 (c) and LTRGO3 (d).

Table 2
XPS elemental analysis of LTRGO samples.

Sample	C/O ratio	O 1s distributions (%)		
		C=O	C-O/C-OH	-COOH
LTRGO1	7.0	51.2	46.0	2.8
LTRGO2	7.2	46.6	42.3	11.1
LTRGO3	7.5	43.8	52.0	4.2

properties of the three SCs (Fig. 5f). In the Nyquist plot, the low-frequency region presents nearly straight line, indicating good double layer capacitive behavior couple with pseudocapacitive behavior. The equivalent series resistance (ESR) is mainly composed of three parts: the intrinsic ohmic resistance (R_s), the interfacial charge transfer (R_{ct}) and Warburg diffusion resistance R_w (Fig. S6, see SI) [49]. In high-frequency range, R_s of these SCs are quite similar, indicating effective reduction degree after the thermal reduction process, consistent with the XRD results. The surface property and the morphology of the electrode can affect the ion diffusion either in the electrolyte or the electrode-electrolyte interface, thus impact the value of R_{ct} and R_w [50]. From the Raman and XPS test, the LTRGO1 indicates highest oxygen-containing functional groups among the LTRGO samples, and the corresponding LTRGO1-SC shows lower R_{ct} and R_w that of other SCs, revealing higher oxygen-containing groups can improve the ion diffusion rate [51]. The total R_{ESR} of 1.99, 3.54 and 4.16 Ω is obtained for the LTRGO1-SC, LTRGO2-SC and LTRGO3-SC (Table S2, see SI), respectively, suggesting the synergistic effect of the conductively and oxygen-containing functional groups is important for performing high specific capacitance for advanced carbon materials with oxygen doped [48].

As known, the energy density in SC is proportional to the square of open circuit voltage, the supercapacitive performance of LTRGO1 have also been tested in 1.0 M Na_2SO_4 aqueous electrolyte, as shown in Fig. 6. To determine the optimal and stable voltage range, CV curves in different ranges are performed. Fig. 6a shows the CV profiles of the symmetric capacitor at 50 mV s^{-1} with in different potential windows. Similar to the case in 6.0 M KOH aqueous electrolyte, the CV curves exhibit a well rectangular-like shape even with the potential shifting to 1.8 V, but with a current increased drastically while further extending the potential to 2.0 V. This result indicates that the electrolyte is not being stable owing to the oxygen and/or hydrogen evolution reaction and the detailed test of the symmetric capacitor are performed in the voltage range of 0–1.8 V [52]. Fig. 6b shows the typical CV curves at different scan rates from 10 to 500 mV s^{-1} and the curves still maintain near rectangular-like shape even with increasing the scan rate to 500 mV s^{-1}, which may be attributed to fast ion charge transfer. Obviously, the CV curves in the whole range of 10–500 mV s^{-1} with no obvious distortion in the anodic current, further indicating that the LTRGO1 are capable of stable operation at voltage up to 1.8 V in 1.0 M Na_2SO_4 aqueous electrolyte. Fig. 6c presents the GCD curves of symmetric SC at various current densities from 0.5 to 20 A g^{-1}, and the linear sharp of the curves in the whole range of current densities indicate excellent electrochemical reversibility. From the discharge curve, the calculated specific capacitance can reach 118 F g^{-1} at a loading current of 0.5 A g^{-1}. As shown in Fig. 6d, the interfacial resistance between the Na_2SO_4 aqueous electrolyte and the LTRGO1 electrode is about 1.02 Ω, demonstrating low electronic resistance. The leakage current of LTRGO1-SC was also investigated, which is

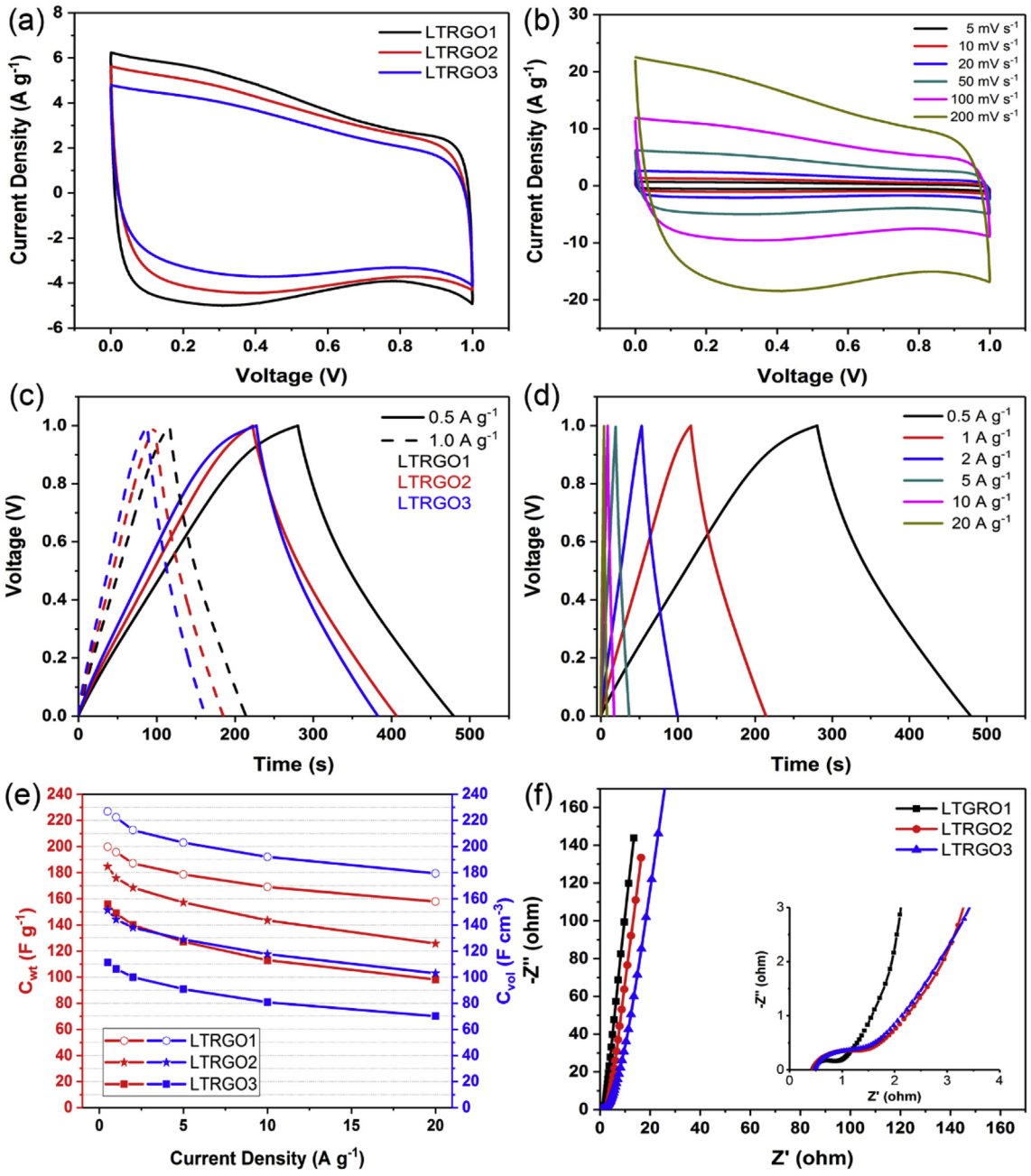

Fig. 5. Supercapacitor performance of LTRGO1-SC, LTRGO2-SC and LTRGO3-SC in 6.0 M KOH electrolyte. (a) CV curves of all SCs at the scan rate of 50 mV s^{-1}; (b) CV curves of LTRGO1-SC at different scan rates ranging from 5 mV s^{-1} to 200 mV s^{-1}; (c) GCD curves of all SCs at the current densities of 0.5 A g^{-1} and 1 A g^{-1}; (d) GCD curves of LTRGO1-SC at different current densities; (e) C_{wt} and C_{vol} versus current density ranging from 0.5 A g^{-1} to 20 A g^{-1} of all SCs and (f) Nyquist plots. Inset shows the high-frequency range.

meaningful in practical application [53–55]. The device was first charged to 1.8 V at 2 mA, and then the voltage was kept at 1.8 V for 2 h to obtain the leakage current curve (Fig. S7, see SI). The currents at thresholds of the LTRGO1-SC is about 0.71 mA/F/V, which is comparable to previous results of supercapacitors in neutral electrolyte (0.45 mA/F/V) [54]. Lastly, we have used two LTRGO1-SCs in series to light up a commercial blue light-emitting-diode (LED, the working potential is about 2.5 V) (Fig. S8, see SI), indicating the practical application of the LTRGO1-SC.

The electrochemical stability of the LTRGO1-SC was also tested by GCD test for 9000 cycles at 5 A g^{-1} as shown in Fig. 7a. The LTRGO1-SC showed 94.2% capacitance retention over 9000 cycles, indicating outstanding electrochemical stability of the device. The Ragon plots of the LTRGO1-SC in different aqueous electrolyte are shown in Fig. 7b. In 6.0 M KOH electrolyte system, LTRGO1-SC delivers a maximum energy density of 7.9 Wh L^{-1} (6.9 Wh kg^{-1}) at a power density of 142 W L^{-1} (125 W kg^{-1}). Additionally, even at a high power density of 5.26 kW kg^{-1}, the LTRGO1-SC can also deliver a high energy density of 6.2 Wh L^{-1} (5.5 Wh kg^{-1}), demonstrating excellent rate capability. In 1.0 M Na_2SO_4 electrolyte system, the maximal energy density of 15.1 Wh L^{-1} (13.3 Wh kg^{-1}) at a power density of 257 W L^{-1} can be obtained owing to the increasing of operating voltage. Such high volumetric energy density is competitive compared to advanced carbon materials in aqueous electrolyte (Table S3, see SI).

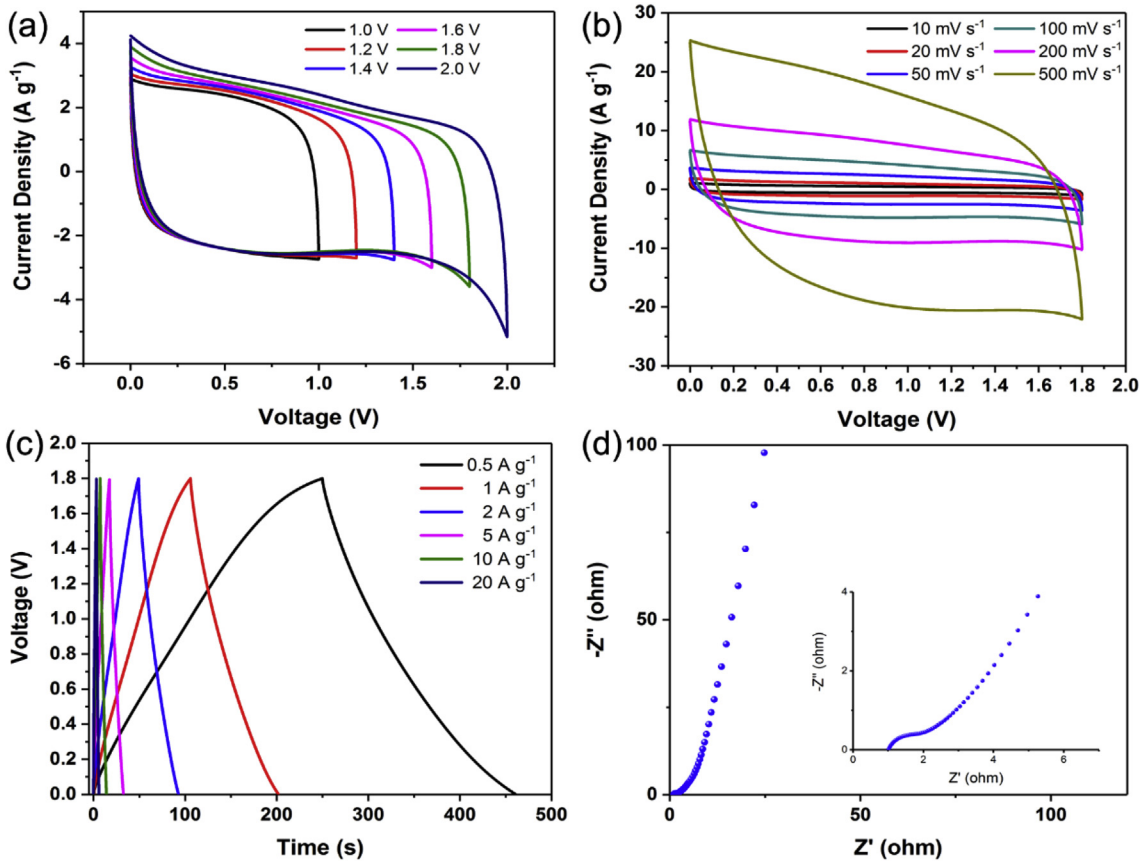

Fig. 6. Electrochemical performance of LTRGO1-SC in 1.0 M Na_2SO_4 electrolyte. (a) CV curves of the cell operated at different voltage ranges at the scan rate of 50 mV s^{-1}; (b) CV curves in 1.8 V at scan rates of 10–500 mV s^{-1}; (c) GCD curves of the cell at various current densities; (d) Nyquist plots. Inset magnifies the high-frequency range.

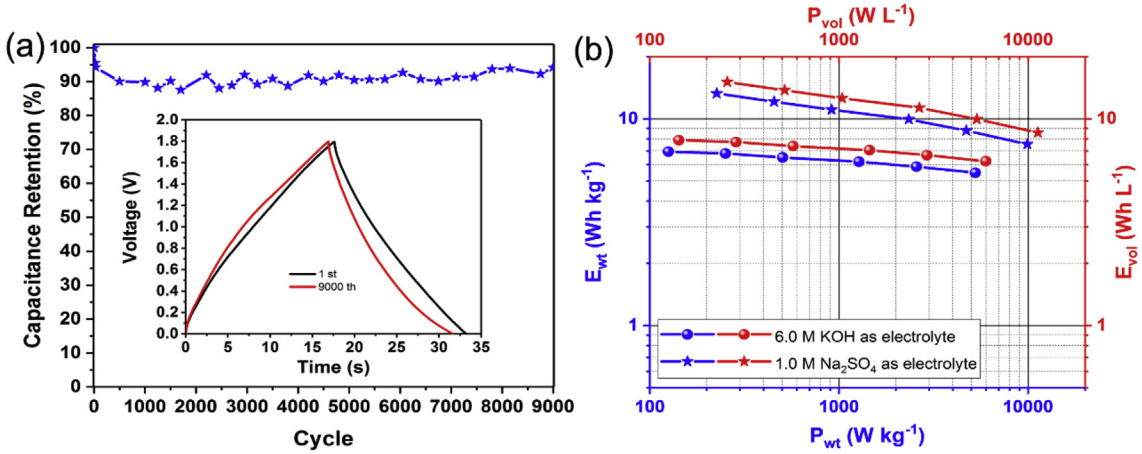

Fig. 7. (a) Cyclic stability of LTRGO1-SC in 1.0 M Na_2SO_4 after nine thousand cycles at 5 A g^{-1} with a voltage window of 1.8 V; (b) Ragone plots of LTRGO1-SC in different aqueous electrolyte.

4. Conclusions

In summary, we have reported a facile, effective and scalable method to prepare funtional graphene with controllable pore structure. This strategy ont only maintains a mass of oxygen-containing funtional groups in the basic plane of graphene, but also controls meso- and macropore volume through using designed particle size of graphite oxide as precursor. Owing to the dense structure and pseudocapacitive functional groups, the as-synthesized LTRGO1-SC displayed high volumetric capacitance 226.9 F cm^{-3} at 0.5 A g^{-1} (7.9 Wh L^{-1}) in 6.0 M KOH electrolyte. While use 1.0 M Na_2SO_4 as electrolyte, a higher volumetric energy density (15.1 Wh L^{-1} at 257 W L^{-1}) as well as a high stability (about 94.2% of capacitance retention after 9000 cycles at 5 A g^{-1}) can be obtained. We believe that the high particle density and functional graphene materials may be a promising material for the applications in catalysis, adsorption, energy storage, etc.

Acknowledgments

This work was supported by the Petro China Innovation Foundation (502000-071100003). We thank Yin Wu for assistance in XRD test and Zuobin Tang for providing microbalance test.

Appendix A. Supplementary data

Supplementary data related to this article can be found at https://doi.org/10.1016/j.electacta.2018.04.034.

References

[1] M.D. Stoller, S. Park, Y. Zhu, J. An, R.S. Ruoff, Graphene-based ultracapacitors, Nano Letters 8 (2008) 3498–3502.
[2] P. Simon, Y. Gogotsi, Materials for electrochemical capacitors, Nat. Mater. 7 (2008) 845.
[3] Y. Bu, S. Tao, Y. Cai, L. Du, Z. Ou, L. Yang, W. Qiang, X. Wang, H. Zheng, Compressing carbon nanocages by capillarity for optimizing porous structures toward ultrahigh-volumetric-performance supercapacitors, Adv. Mater. 29 (2017), 1700470.
[4] H.A. Andreas, B.E. Conway, Examination of the double-layer capacitance of an high specific-area C-cloth electrode as titrated from acidic to alkaline pHs, Electrochim. Acta 51 (2006) 6510–6520.
[5] D. Hulicova-Jurcakova, A.M. Puziy, O.I. Poddubnaya, F. Suárez-García, J.M.D. Tascón, G.Q. Lu, Highly stable performance of supercapacitors from phosphorus-enriched carbons, J. Am. Chem. Soc. 131 (2009) 5026–5027.
[6] D. Sheberla, J.C. Bachman, J.S. Elias, C.J. Sun, Y. Shao-Horn, M. Dincă, Conductive MOF electrodes for stable supercapacitors with high areal capacitance, Nat. Mater. 16 (2017) 220.
[7] N.S. Choi, Z. Chen, S.A. Freunberger, X. Ji, Y.K. Sun, K. Amine, G. Yushin, L.F. Nazar, J. Cho, P.G. Bruce, Challenges facing lithium batteries and electrical double-layer capacitors, Angew Chem. Int. Ed. Engl. 51 (2012) 9994–10024.
[8] L.L. Zhang, X.S. Zhao, Carbon-based materials as supercapacitor electrodes, Chem. Soc. Rev. 38 (2009) 2520–2531.
[9] Y. Fang, B. Luo, Y. Jia, X. Li, B. Wang, Q. Song, F. Kang, L. Zhi, Renewing functionalized graphene as electrodes for high-performance supercapacitors, Adv. Mater. 24 (2012) 6348–6355.
[10] Z. Lei, J. Zhang, L.L. Zhang, N.A. Kumar, X.S. Zhao, Functionalization of chemically derived graphene for improving its electrocapacitive energy storage properties, Energy Environ. Sci. 9 (2016) 1891–1930.
[11] Z. Yu, L. Tetard, L. Zhai, J. Thomas, Supercapacitor electrode materials: nanostructures from 0 to 3 dimensions, Energy Environ. Sci. 8 (2015) 702–730.
[12] R. Raccichini, A. Varzi, S. Passerini, B. Scrosati, The role of graphene for electrochemical energy storage, Nat. Mater. 14 (2015) 271–279.
[13] U. Patil, S.C. Lee, S. Kulkarni, J.S. Sohn, M.S. Nam, S. Han, S.C. Jun, Nanostructured pseudocapacitive materials decorated 3D graphene foam electrodes for next generation supercapacitors, Nanoscale 7 (2015) 6999–7021.
[14] J. Yan, T. Wei, Z. Fan, W. Qian, M. Zhang, X. Shen, F. Wei, Preparation of graphene nanosheet/carbon nanotube/polyaniline composite as electrode material for supercapacitors, J. Power Sources 195 (2010) 3041–3045.
[15] H.-P. Cong, X.-C. Ren, P. Wang, S.-H. Yu, Flexible graphene–polyaniline composite paper for high-performance supercapacitor, Energy Environ. Sci. 6 (2013) 1185.
[16] Y. Yan, B. Li, W. Guo, H. Pang, H. Xue, Vanadium based materials as electrode materials for high performance supercapacitors, J. Power Sources 329 (2016) 148–169.
[17] Z.S. Wu, D.W. Wang, W. Ren, J. Zhao, G. Zhou, F. Li, H.M. Cheng, Anchoring hydrous RuO2 on graphene sheets for high-performance electrochemical capacitors, Adv. Funct. Mater. 20 (2010) 3595–3602.
[18] S. Chen, J. Zhu, X. Wu, Q. Han, X. Wang, Graphene Oxide–MnO2 nanocomposites for supercapacitors, ACS Nano 4 (2010) 2822–2830.
[19] G. Lota, E. Frackowiak, Pseudocapacitance effects for enhancement of capacitor performance, Fuel Cell. 10 (2010) 848–855.
[20] F. Liu, D. Xue, An electrochemical route to quantitative oxidation of graphene frameworks with controllable C/O ratios and added pseudocapacitances, Chem. Eur J. 19 (2013) 10716–10722.
[21] X. Wu, D. Yang, C. Wang, Y. Jiang, T. Wei, Z. Fan, Functionalized three-dimensional graphene networks for high performance supercapacitors, Carbon 92 (2015) 26–30.
[22] C. Zhang, W. Lv, Y. Tao, Q.-H. Yang, Towards superior volumetric performance: design and preparation of novel carbon materials for energy storage, Energy Environ. Sci. 8 (2015) 1390–1403.
[23] Q. Wang, J. Yan, Z. Fan, Carbon materials for high volumetric performance supercapacitors: design, progress, challenges and opportunities, Energy Environ. Sci. 9 (2016) 729–762.
[24] J. Yan, Q. Wang, T. Wei, L. Jiang, M. Zhang, X. Jing, Z. Fan, Template-assisted low temperature synthesis of functionalized graphene for ultrahigh volumetric performance supercapacitors, ACS Nano 8 (2014) 4720–4729.
[25] X. Yang, C. Cheng, Y. Wang, L. Qiu, D. Li, Liquid-mediated dense integration of graphene materials for compact capacitive energy storage, Science 341 (2013) 534–537.
[26] H. Li, Y. Tao, X. Zheng, J. Luo, F. Kang, H.-M. Cheng, Q.-H. Yang, Ultra-thick graphene bulk supercapacitor electrodes for compact energy storage, Energy Environ. Sci. 9 (2016) 3135–3142.
[27] X. Dong, N. Hu, L. Wei, Y. Su, H. Wei, L. Yao, X. Li, Y. Zhang, A new strategy to prepare N-doped holey graphene for high-volumetric supercapacitors, J. Mater. Chem. A 4 (2016) 9739–9743.
[28] J. Li, K. Liu, X. Gao, B. Yao, K. Huo, Y. Cheng, X. Cheng, D. Chen, B. Wang, W. Sun, D. Ding, M. Liu, L. Huang, Oxygen- and nitrogen-enriched 3D porous carbon for supercapacitors of high volumetric capacity, ACS Appl. Mater. Interfaces 7 (2015) 24622–24628.
[29] Y. Zhang, L. Ji, W. Li, Z. Zhang, L. Lu, L. Zhou, J. Liu, Y. Chen, L. Liu, W. Chen, Y. Zhang, Highly defective graphite for scalable synthesis of nitrogen doped holey graphene with high volumetric capacitance, J. Power Sources 334 (2016) 104–111.
[30] B. Liu, Y. Liu, H. Chen, M. Yang, H. Li, Oxygen and nitrogen co-doped porous carbon nanosheets derived from Perilla frutescens for high volumetric performance supercapacitors, J. Power Sources 341 (2017) 309–317.
[31] N.P. Sari, D. Dutta, A. Jamaluddin, J.-K. Chang, C.-Y. Su, Controlled multimodal hierarchically porous electrode self-assembly of electrochemically exfoliated graphene for fully solid-state flexible supercapacitor, Phys. Chem. Chem. Phys. 19 (2017) 30381–30392.
[32] Y. Xu, C.-Y. Chen, Z. Zhao, Z. Lin, C. Lee, X. Xu, C. Wang, Y. Huang, M.I. Shakir, X. Duan, Solution processable holey graphene oxide and its derived macrostructures for high-performance supercapacitors, Nano Letters 15 (2015) 4605–4610.
[33] S.M. Jung, D.L. Mafra, C.-T. Lin, H.Y. Jung, J. Kong, Controlled porous structures of graphene aerogels and their effect on supercapacitor performance, Nanoscale 7 (2015) 4386–4393.
[34] J.-H. Chang, Y.-H. Hung, X.-F. Luo, C.-H. Huang, S. Jung, J.-K. Chang, J. Kong, C.-Y. Su, The hierarchical porosity of a three-dimensional graphene electrode for binder-free and high performance supercapacitors, RSC Adv. 6 (2016) 8384–8394.
[35] W. Gao, J. Li, X. Yan, B. Zhu, J. Jia, A. Huang, K. Xie, Y. Bai, Accordion-like graphene by a facile and green synthesis method reinforcing polyolefin nanocomposites, RSC Adv. 7 (2017) 31085–31092.
[36] D.R. Dreyer, S. Park, C.W. Bielawski, R.S. Ruoff, The chemistry of graphene oxide, Chem. Soc. Rev. 39 (2010) 228–240.
[37] S.J. Yang, T. Kim, H. Jung, C.R. Park, The effect of heating rate on porosity production during the low temperature reduction of graphite oxide, Carbon 53 (2013) 73–80.
[38] A.C. Ferrari, J.C. Meyer, V. Scardaci, C. Casiraghi, M. Lazzeri, F. Mauri, S. Piscanec, D. Jiang, K.S. Novoselov, S. Roth, A.K. Geim, Raman spectrum of graphene and graphene layers, Phys. Rev. Lett. 97 (2006), 187401.
[39] S.B. Yoon, G.S. Chai, S.K. Kang, J.-S. Yu, K.P. Gierszal, M. Jaroniec, Graphitized pitch-based carbons with ordered nanopores synthesized by using colloidal crystals as templates, J. Am. Chem. Soc. 127 (2005) 4188–4189.
[40] M.M. Lucchese, F. Stavale, E.H.M. Ferreira, C. Vilani, M.V.O. Moutinho, R.B. Capaz, C.A. Achete, A. Jorio, Quantifying ion-induced defects and Raman relaxation length in graphene, Carbon 48 (2010) 1592–1597.
[41] J. Schwan, S. Ulrich, V. Batori, H. Ehrhardt, S.R.P. Silva, Raman spectroscopy on amorphous carbon films, J. Appl. Phys. 80 (1996) 440–447.
[42] Z. Liu, K. Xiao, H. Guo, X. Ning, A. Hu, Q. Tang, B. Fan, Y. Zhu, X. Chen, Nitrogen-doped worm-like graphitized hierarchical porous carbon designed for enhancing area-normalized capacitance of electrical double layer supercapacitors, Carbon 117 (2017) 163–173.
[43] A. Sadezky, H. Muckenhuber, H. Grothe, R. Niessner, U. Pöschl, Raman microspectroscopy of soot and related carbonaceous materials: spectral analysis and structural information, Carbon 43 (2005) 1731–1742.
[44] J.C. Groen, L.A.A. Peffer, J. Pérez-Ramırez, Pore size determination in modified micro- and mesoporous materials. Pitfalls and limitations in gas adsorption data analysis, Microporous Mesoporous Mater. 60 (2003) 1–17.
[45] R. Arrigo, M. Hävecker, S. Wrabetz, R. Blume, M. Lerch, J. McGregor, E.P.J. Parrott, J.A. Zeitler, L.F. Gladden, A. Knop-Gericke, R. Schlögl, D.S. Su, Tuning the acid/base properties of nanocarbons by functionalization via amination, J. Am. Chem. Soc. 132 (2010) 9616–9630.
[46] D. Hulicova-Jurcakova, M. Seredych, G.Q. Lu, T.J. Bandosz, Combined effect of nitrogen- and oxygen-containing functional groups of microporous activated carbon on its electrochemical performance in supercapacitors, Adv. Funct. Mater. 19 (2009) 438–447.
[47] E. Frackowiak, F. Béguin, Carbon materials for the electrochemical storage of energy in capacitors, Carbon 39 (2001) 937–950.
[48] L. Jiang, L. Sheng, C. Long, T. Wei, Z. Fan, Functional pillared graphene frameworks for ultrahigh volumetric performance supercapacitors, Adv. Energy Mater. 5 (2015), 1500771.
[49] J. Zhao, Y. Jiang, H. Fan, M. Liu, O. Zhuo, X. Wang, Q. Wu, L. Yang, Y. Ma, Z. Hu, Porous 3D few-layer graphene-like carbon for ultrahigh-power supercapacitors with well-defined structure–performance relationship, Adv. Mater. 29 (2017), 1604569.
[50] J. Gamby, P.L. Taberna, P. Simon, J.F. Fauvarque, M. Chesneau, Studies and characterisations of various activated carbons used for carbon/carbon supercapacitors, J. Power Sources 101 (2001) 109–116.
[51] J. Chang, Z. Gao, X. Liu, D. Wu, F. Xu, Y. Guo, Y. Guo, K. Jiang, Hierarchically porous carbons with graphene incorporation for efficient supercapacitors, Electrochim. Acta 213 (2016) 382–392.

[52] Q. Wang, J. Yan, Y. Wang, T. Wei, M. Zhang, X. Jing, Z. Fan, Three-dimensional flower-like and hierarchical porous carbon materials as high-rate performance electrodes for supercapacitors, Carbon 67 (2014) 119–127.
[53] A.B. Fuertes, G. Lota, T.A. Centeno, E. Frackowiak, Templated mesoporous carbons for supercapacitor application, Electrochim. Acta 50 (2005) 2799–2805.
[54] W. Quan, C. Jiang, S. Wang, Y. Li, Z. Zhang, Z. Tang, F. Favier, New nanocomposite material as supercapacitor electrode prepared via restacking of Ni-Mn LDH and MnO2 nanosheets, Electrochim. Acta 247 (2017) 1072–1079.
[55] L. Chen, H. Bai, Z. Huang, L. Li, Mechanism investigation and suppression of self-discharge in active electrolyte enhanced supercapacitors, Energy Environ. Sci. 7 (2014) 1750–1759.